Hindawi
International Journal of Polymer Science
Volume 2017, Article ID 7804743, 15 pages
https://doi.org/10.1155/2017/7804743

Research Article

CO_2 Induced Foaming Behavior of Polystyrene near the Glass Transition

Salah Al-Enezi

Petroleum Research Centre, Kuwait Institute for Scientific Research, Safat, Kuwait

Correspondence should be addressed to Salah Al-Enezi; senezi@kisr.edu.kw

Received 14 May 2017; Revised 20 July 2017; Accepted 17 September 2017; Published 17 October 2017

Academic Editor: Miriam H. Rafailovich

This paper examines the effect of high-pressure carbon dioxide on the foaming process in polystyrene near the glass transition temperature and the foaming was studied using cylindrical high-pressure view cell with two optical windows. This technique has potential applications in the shape foaming of polymers at lower temperatures, dye impregnation, and the foaming of polystyrene. Three sets of experiments were carried out at operating temperatures of 50, 70, and 100°C, each over a range of pressures from 24 to 120 bar. Foaming was not observed when the polymer was initially at conditions below T_g but was observed above T_g. The nucleation appeared to occur randomly leading to subsequent bubble growth from these sites, with maximum radius of 0.02–0.83 mm. Three models were applied on the foaming experimental data. Variable diffusivity and viscosity model (Model C) was applied to assess the experimental data with the WLF equation. The model shows very good agreement by using realistic parameter values. The expansion occurs by diffusion of a dissolved gas from the supersaturated polymer envelope into the bubble.

1. Introduction

The use of high-pressure carbon dioxide as an efficient medium for polymer processing due to its chemical and economic advantages [1–3]. The unique properties associated with CO_2 have been explored for a long time in fields of polymer processing as they lower the glass transition temperature. In foaming process, the polymer is saturated with CO_2 in the supercritical state followed by equilibrium swelling state. After saturation, the sample transformed into a rubbery state and depressurized to atmospheric pressure to take the advantage of the swelling and plasticization of the polymer, which reduces the glass transition temperature (T_g) or melting temperature (T_m) due to its high solubility in polymers [4]. The chemical structure of polymers greatly impacts CO_2 solubility and diffusivity. The CO_2-philic groups such as carbonyl or ether groups in the backbone or on side chains of a polymer interact with CO_2 and help with the dissolution of CO_2 within the polymer [5, 6]. Gas foaming is one of the most generally used techniques for the fabrication of porous polymers and the use of supercritical CO_2 for generating porous polymeric foams has generated significant interest over the years [7–10]. The bubble growth data are important for understanding the foam growth. Recently many researchers investigated the effect of pressure drop rate (PDR) on the foam morphology, density, and cell size distribution in nanocellular foams [11–13]. It is important to note that an increase of the PDR increases the rate of stable nuclei formation, at the same time reducing the chances for the foaming agent to fill the freshly formed bubbles [13]. Bubble formation and foaming are caused by CO_2, earlier dissolved in the polymer under pressure, to be released upon depressurization. This has been well reported in the literature and a number of models for bubble growth have been presented by many authors [14–18]. The bubble growth data are important for understanding the foam growth. Foam modelling can by divided into three stages: bubble nucleation, bubble growth, and possibly coarsening. Bubble growth is the most thoroughly studied of the three. Many models have been proposed for radial growth of a single bubble in an infinite expanse of melt, and most of the models are similar. Viscosity, diffusivity, and surface tension are potentially significant to foaming. All three factors directly affect the growth of gas bubbles and therefore will have an impact on the bubble-size and ultimate properties of the foamed product [16].

In this paper, the bubble radius of polystyrene/CO_2 is measured in situ using a specially constructed high-pressure view cell with 2 optical windows, connected to a digital

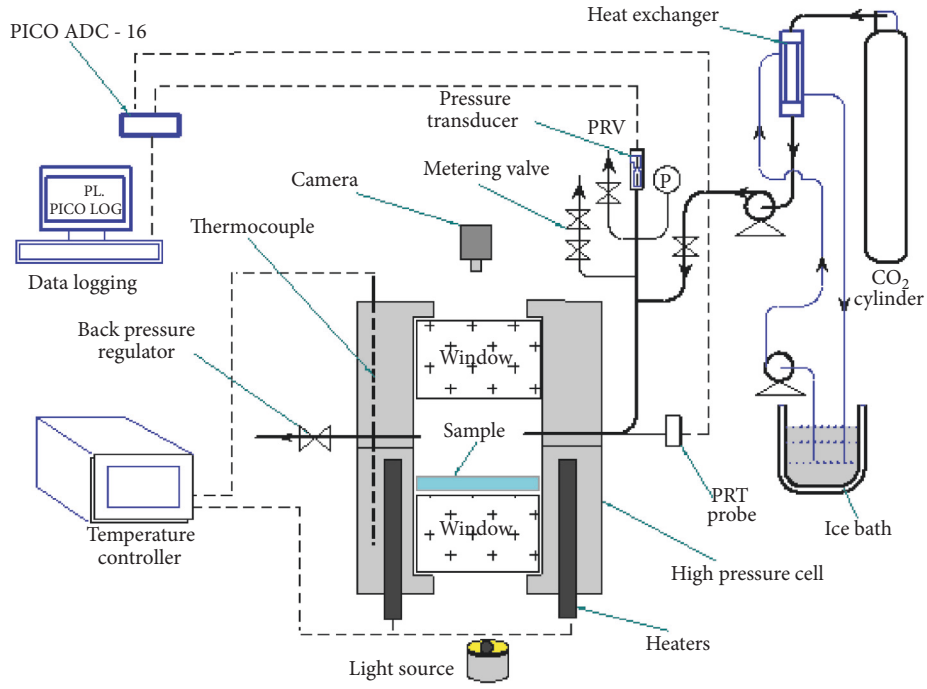

Figure 1: Experimental set-up showing connections to the viewing cell.

still camera with a high magnification lens to monitor and record the bubbles growing, to compare the results against bubble growth models. The experimental data are analysed by measuring bubble radii at different times using image analysis software. In the present work, three foam models were applied along with foaming experimental data. Model C was mainly applied to assess the variation of viscosity and diffusivity model with the WLF equation.

2. Methods and Materials

The polystyrene (Mw 184,000 g/mol, T_g 102.6°C) sheets with a thickness of 1 mm were obtained from Polybron Ltd., UK. The disc shaped test samples with a diameter of 20 mm are cut from the sheet using specimen cutting machine Charly4U. The pressure view cell is specially designed to investigate polystyrene, PS foaming, and bubble growth. The cylindrical cell was constructed from 316 stainless steel (with dimensions of 95 mm height and 65 mm diameter) with two window ports incorporated so that the sample can be continuously viewed through one window whilst using the second window for illumination (Figure 1).

The cell has high-pressure connections to work as inlet and outlet ports for CO_2 transfer. Each window has two O-rings (silicon ring can work up 200°C), one in the face and one for radial sealing. The cell was made in two sections and can be opened from the center. Around the sample there are three heating cartridges and a thermocouple fitted in the wall of the cell. With this cell it is also possible to control and record all pressure and temperature data during an experiment and at the same time obtain digital pictures of the experiments progress. The heaters are heated up to a temperature of 600°C.

The experimental procedure was performed according to the following method:

(a) The polymer sample was placed in the cell; then the cell was sealed.

(b) Carbon dioxide was introduced into the cell from a supply cylinder, using a pump where necessary to reach the desired pressure.

(c) Isothermal tests were performed at 70 and 100°C with different pressure range (24, 44, 63, 83, 100, and 120 bar) for 2 hours; each test was done in a separate experiment.

(d) Heating was then stopped and the cell depressurized over the course of 3 minutes.

(e) The bubble nucleation and growth were recorded by the optical microscope and digital camera (1 frame/3 sec).

(f) After the cell had completely cooled, the samples were removed.

(g) The bubble radius was then analysed by image analysis software (Image-J).

3. Results and Analyses

3.1. Effect of Conditioning Time. Experiments were performed on disk samples (1 mm) and diameter (20 mm) with

Figure 2: Photographs of samples of PS depressurized after holding for different times (30 to 180 min) at 100°C and 54 bar (1 mm thickness × 20 mm diameter).

different conditioning times of 30, 60, 120, 160, and 180 minutes with the same pressure (54 bar) and temperature (100°C), and the corresponding photographs of the depressurized samples were showed in Figure 2. This was in order to assess the time required for CO_2 to satisfactorily equilibrate in the sample prior to depressurization. As the conditioning time is increased up to 120 minutes, it can be seen that the radius of the foamed sample increases and there is less interstitial space between the bubbles. Both indicate a greater bubble volume as the conditioning time is increased. This must be caused by more CO_2 diffusing into the sample at the longer conditioning times indicating that the 30 minutes and 60 minutes times are insufficient to allow equilibration of CO_2 in the sample to occur. Sample conditioned at 120 min achieved maximum bubble foaming. It can also be seen that the 160- and 180-minute sample grew almost to the same size with notable color change due to degradation compared to the 120-minute sample. Therefore, it was decided that the 120-minute conditioning time was sufficient for our experiments.

3.2. Effect of Impingement. During the analysis of the bubble growth data, it was found that bubbles in the samples grow at different rates according to the proximity of other bubbles. One sample has been selected as an example, 24 bar and 100°C, to illustrate this effect. The following photo has been taken after 600 seconds at 0 bar (Figure 3) and shows four bubbles, one of which is "free" and the others are touching each other.

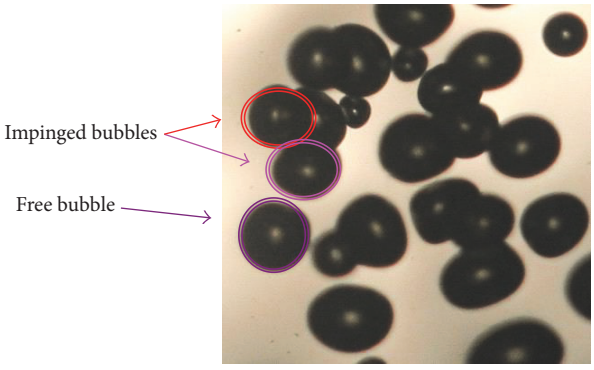

Figure 3: Photograph of a PS (1 mm thick × 20 mm diameter) sample 600 sec after the onset of depressurization after holding at 24 bar (CO_2 pressure) and 100°C for 2 hours, the photograph shows the location of three impinged bubbles and one free bubble that are considered here (scale of images is 6 × 6 mm).

3.3. Conditions Effect of Pressure and Temperature. Three main operating temperatures were selected (50, 70, and 100°C) each over a range of pressures from 24 to 120 bar. For the 100°C experiments, the polymer will be in the

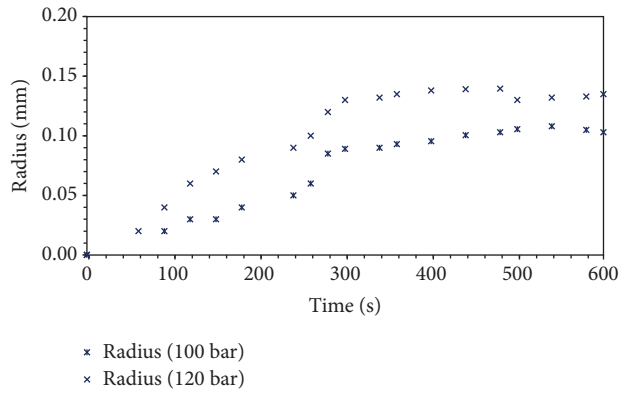

FIGURE 4: Bubble radius of PS/CO_2 during depressurization after holding at 100 and 120 bar at 50°C for 2 hours.

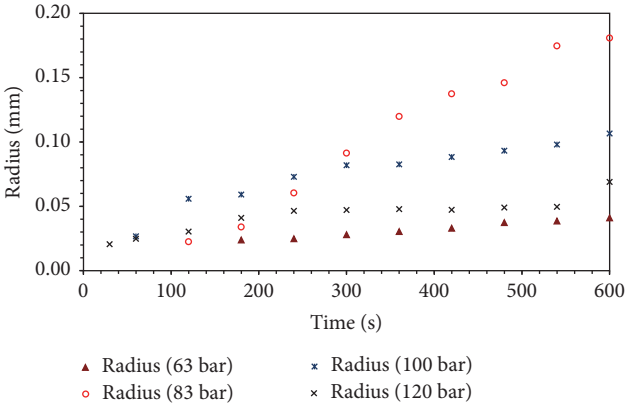

FIGURE 5: Bubble radius of PS/CO_2 during depressurization after holding at 63 to 120 bar at 70°C for 2 hours.

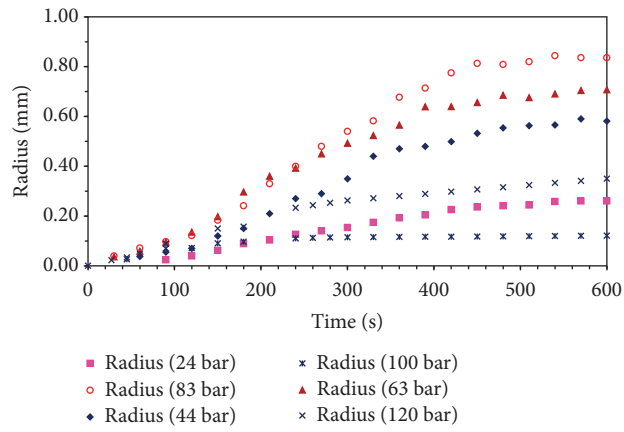

FIGURE 6: Bubble radius of PS/CO_2 during depressurization after holding at 24 to 120 bar at 100°C for 2 hours.

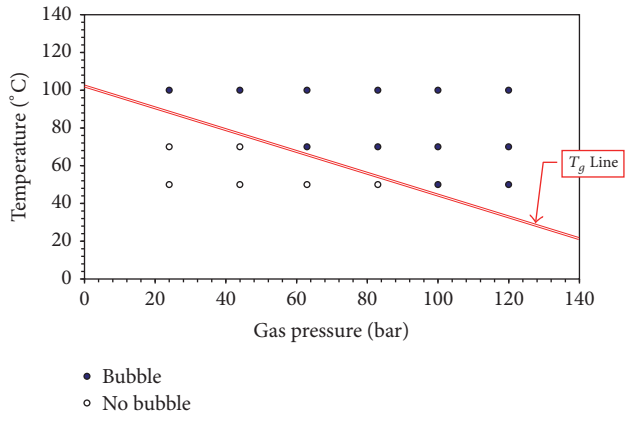

FIGURE 7: Incident of bubble formation and T_g line.

rubbery state at the onset of depressurization and much of the subsequent time period. However, most of the 50°C experiments (below 100 bar) and 70°C experiments (below 63 bar) will be with the polymer entirely within the glassy state.

Depressurization experiments at 50°C and 70°C up at low pressure show no sign of any bubble formation. These correspond to conditions below T_g of PS. However, at higher pressures for 50°C and 70°C bubbles start to appear after 30 sec, with maximum radius of 0.02–0.18 as the radius calculation shown in Figures 4 and 5. The third set of experiments was performed at a higher temperature (100°C) (above T_g of PS) up to 120 bar; see Figure 6. These conditions coincided with those for which literature data for diffusivity and Henry's law constants were available. These experiments were carried out in the view cell and the photographs of specimens during different stages of the experiment were analysed using image analysis software to provide data for bubble radius versus time.

These measurements were performed at a higher temperature condition of 100°C and pressure ranges of 24 to 120 bar. Thus, all samples are initially in the rubbery state (above T_g). Bubbles appeared in all the experiments without exception. The nucleation appeared to occur randomly leading to subsequent bubble growth from these sites. With time, more bubbles nucleate and grow, and the bubbles initially appear to be circular. As more bubbles form and grow in close proximity to each other, their shape is influenced by the impingement of surrounding neighbours leading to polygon shaped bubbles towards the end, with each bubble separated from the neighbouring bubble by a thin film of polymer.

3.4. Incidence of Bubble Formation. At low temperature, there were no signs of bubble formation which is corresponding to the glassy state of PS. However, at high pressures and temperatures above T_g, nucleation occurred. Figure 7 illustrates these incidents of bubble formation for all the operating conditions. The results also compared with the reported values of plasticization of PS by high-pressure CO_2 [20]. It can be clearly seen that bubbles form only when the polymer has been in the rubbery state.

3.5. Possible Influence of the Glass Transition on Bubble Growth. It has been noted from the previous investigation in this work that T_g has the biggest influence on bubble growth. In Figure 8 (at the experimental condition of 24 bar

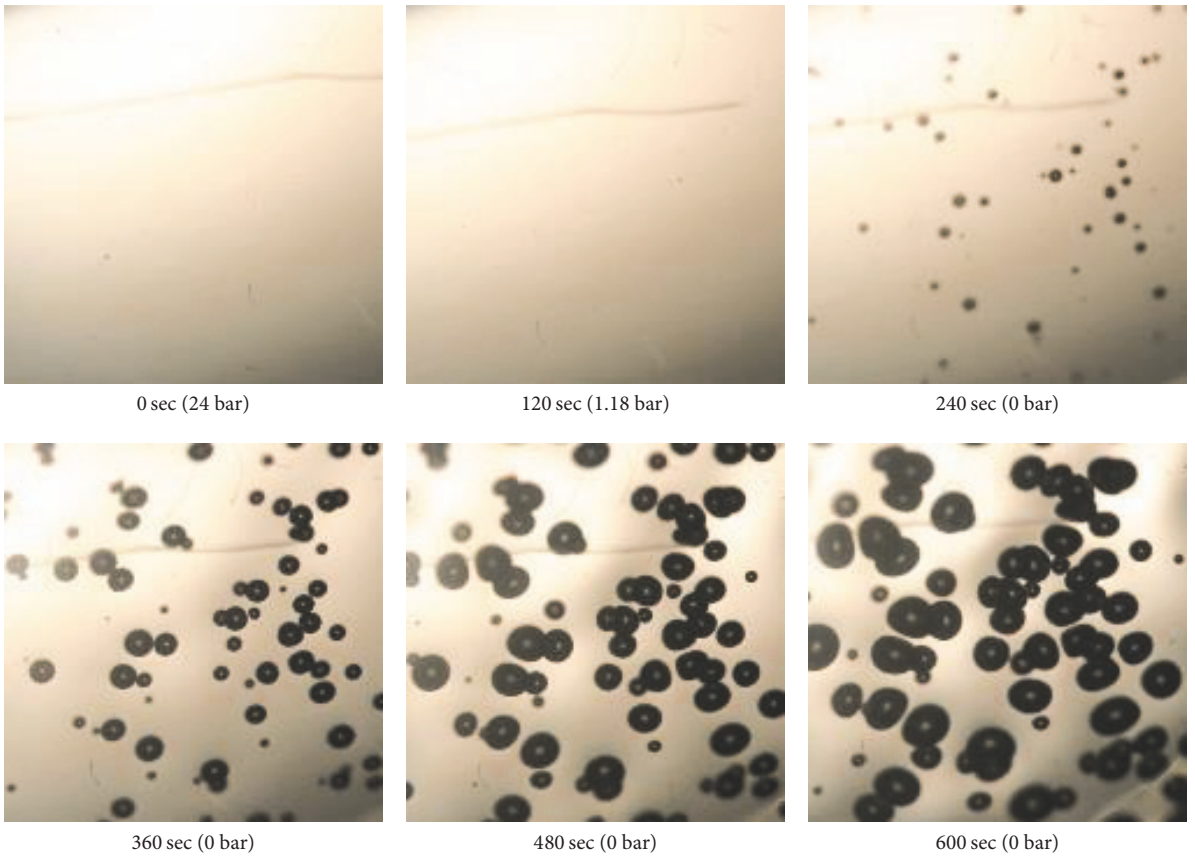

Figure 8: Photographs of a 1 mm thick PS sample at various times after the onset of depressurization after holding at 24 bar (in CO_2) and 100°C for 2 hours (scale of images is 6 × 6 mm).

and 100°C), it can be seen that the bubbles grow very freely without impinging but that the growth stops after 480 seconds before impingement occurred, which indicate that the growth here is not limited by impingement. Another experiment also showed that the sorption and diffusion of CO_2 cannot be used as a predictor of bubble growth. At the experimental conditions at 83 bar and the two different temperatures of 70°C (Figure 9) and 100°C (Figure 10), it was found that the bubble diameter at 70°C is much smaller than at 100°C. As the temperature rises, the viscosity falls which aids foaming. When CO_2 diffuses into a polymer, the polymer swells and the density of the polymer/CO_2 system reduces. Generally diffusion of carbon dioxide results in a strong plasticization effect for a number of polymers. It is also obvious that bubbles do not expand freely such that the CO_2 bubble pressure equilibrates with the cell pressure as this would result in much larger foam volumes than what are observed. It is thus likely that bubble growth reduces as the polymer (at some point) passes from the rubbery to the glassy state.

3.6. Pressure Depressurization Curves. Figure 11 illustrates the depressurization curves for all the experiments performed at 100°C. All the experiments reached 0 bar before 300 sec of depressurization. With low pressure (24 to 44 bar), the time to reach 0 bar was between 175 and 200 sec and for the high pressure (85 to 120 bar) it was around 275 to 300 sec. This is because the low pressure experiments have less gas to evacuate from the cell. We can see from all the previous Figures 4–6 that the bubbles keep growing even when the cell pressure has reached 0 bar, and some bubbles start to appear even after this time in the interstices between the bubbles. This trend happens at all pressures but it can be seen more clearly with the higher pressures. This shows that the CO_2 in the polymer, in the bubbles, and in the surrounding gas is not in equilibrium. In 100°C experiments the temperature is above the glass transition; therefore, the polymer is in the rubbery phase and the bubbles can grow very easily which made the bubbles very big compared with the earlier investigations in this work.

3.7. Bubble Growth Modelling

3.7.1. Model Framework. This model is to be used to fit to experimental data of bubble growth. The general model framework uses a finite difference technique as illustrated in Figure 12. The bubble, assumed to contain pure CO_2, is surrounded by a polymer sphere which is divided into 20 concentric shells of equal volume.

The polymer density is assumed to be constant, and hence the volumes associated with each shell remain constant. Therefore, knowledge of the current bubble radius at any time allows all the nodal radii to be evaluated.

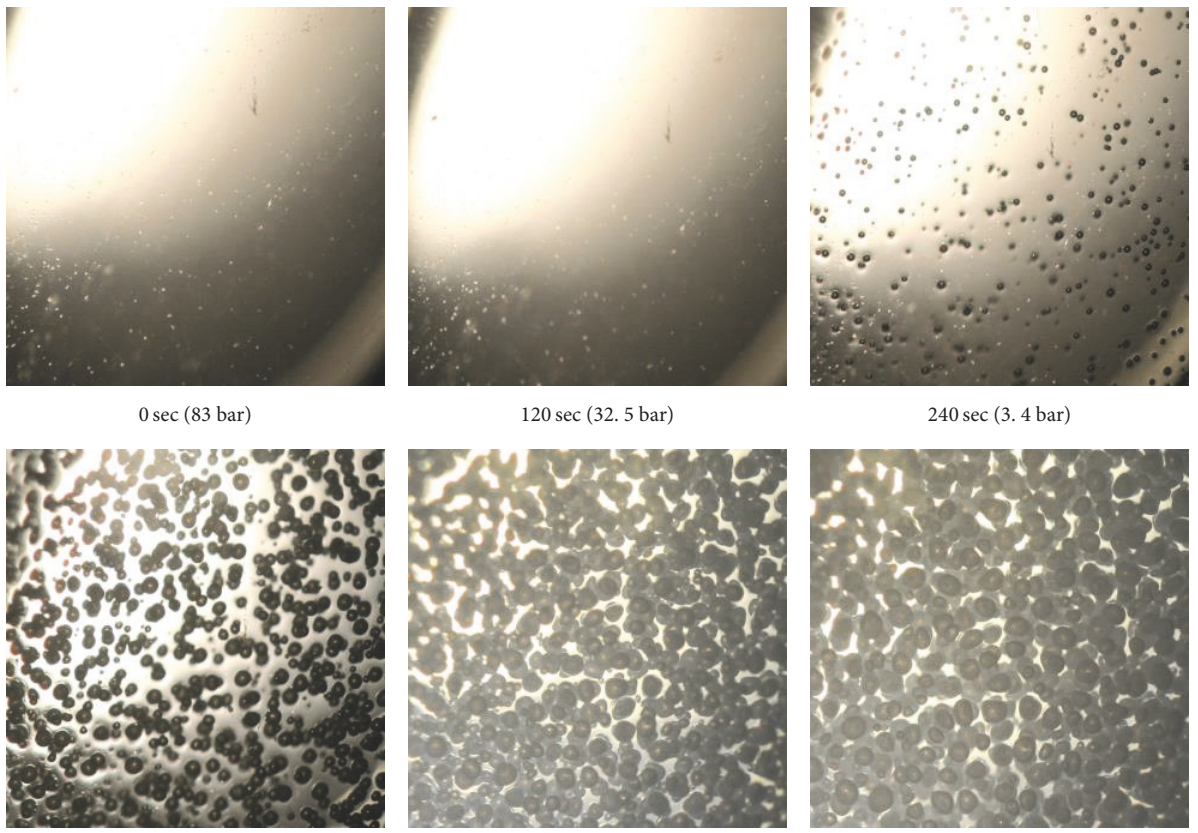

Figure 9: Photographs of a 1 mm thick PS sample at various times after the onset of depressurization after holding at 83 bar (in CO_2) and 70°C for 2 hours (scale of images is 6 × 6 mm).

$$\frac{4}{3}\pi r_a^3 + fV_{\text{polymer}} = \frac{4}{3}\pi r^3, \tag{1}$$

where V_{polymer} is the volume of polymer, f is the fraction of polymer volume inside the nodal radius, r_a is radius at node "a," and r is the radius at the node.

3.7.2. Diffusion Equations. Different equations are required to model concentrations at the bubble interface (node "a") and exterior (node "u") and within the polymer (nodes "b" to "t").

Main Body (Nodes "b" to "t"). Here node "q" is used as an example node for explanatory purposes with adjacent nodes "r" (outside) and "p" (inside). Equations for other nodes are essentially identical.

The volume associated with node "q" is a shell with outer radius $(1/2)(r_q + r_r)$ and inner radius $(1/2)(r_q + r_p)$.

$$\begin{aligned}
&\text{Flux In} = D_{qr}\frac{(c_r - c_q)}{(r_r - r_q)} \quad (\text{From node "}r\text{"}),\\
&\text{Area} = 4\pi\left(\frac{r_q + r_r}{2}\right)^2 \quad \text{of "}q, r\text{" boundary},
\end{aligned} \tag{2}$$

$$\begin{aligned}
&\text{Flux Out} = D_{qp}\frac{(c_q - c_p)}{(r_q - r_p)} \quad (\text{to node "}p\text{"}),\\
&\text{Area} = 4\pi\left(\frac{r_q + r_p}{2}\right)^2 \quad \text{of "}q, p\text{" boundary},
\end{aligned} \tag{3}$$

$$\text{Accumulation} = \frac{dc_q}{dt} \times \text{Volume}, \tag{4}$$

$$\text{Volume} = \frac{4}{3}\pi\left(\frac{r_q + r_r}{2}\right)^3 - \frac{4}{3}\pi\left(\frac{r_q + r_p}{2}\right)^3, \tag{5}$$

$$\text{Accumulation} = \text{Flux in} \times \text{Area} - \text{Flux out} \times \text{Area},$$

$$\begin{aligned}
&\frac{dc_q}{dt}\frac{4}{3}\pi\left[\left(\frac{r_q + r_r}{2}\right)^3 - \left(\frac{r_q + r_p}{2}\right)^3\right]\\
&\quad = 4\pi\left(\frac{r_q + r_r}{2}\right)^2 D_{qr}\frac{(c_r - c_q)}{(r_r - r_q)}\\
&\qquad - 4\pi\left(\frac{r_q + r_p}{2}\right)^2 D_{qp}\frac{(c_q - c_p)}{(r_q - r_p)}.
\end{aligned} \tag{6}$$

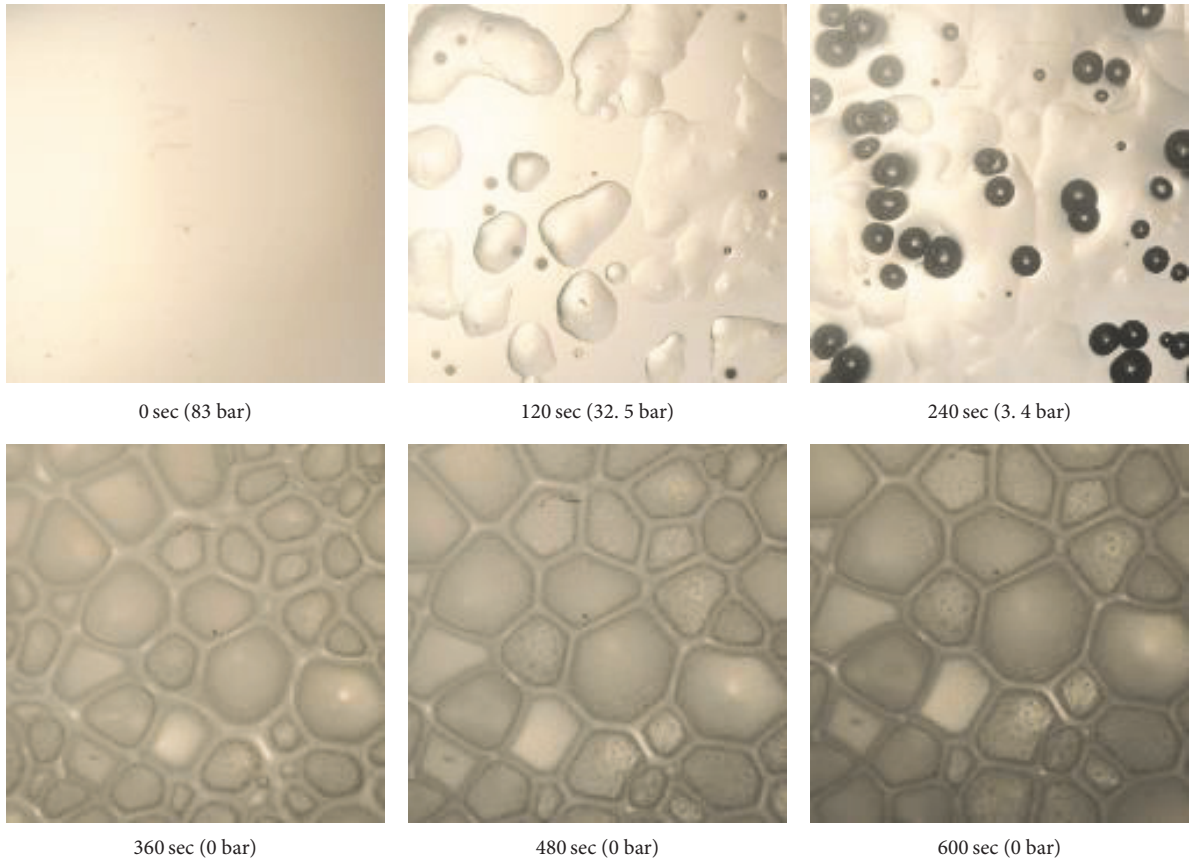

FIGURE 10: Photographs of a 1 mm thick PS sample at various times after the onset of depressurization after holding at 83 bar (in CO_2) and 100°C for 2 hours (scale of images is 6 × 6 mm).

Cancelling π,

$$\frac{dc_q}{dt}\frac{1}{6}\left[\left(r_q+r_r\right)^3-\left(r_q+r_p\right)^3\right] = \left(r_q+r_r\right)^2 D_{qr}\left(\frac{c_r-c_q}{r_r-r_q}\right) - \left(r_q+r_p\right)^2 D_{qp}\left(\frac{c_q-c_p}{r_q-r_p}\right). \quad (7)$$

Exterior Boundary (No Flux): Node "u." One has

$$\text{Flux Out} = D_{tu}\frac{\left(c_u-c_t\right)}{\left(r_u-r_t\right)} \quad \text{(to node "}t\text{")},$$

$$\text{Area} = 4\pi\left(\frac{r_t+r_u}{2}\right)^2 \quad \text{of "}q,r\text{" boundary},$$

$$\text{Accumulation} = \frac{dc_u}{dt}\times \text{Volume},$$

$$\text{Volume} = \frac{4}{3}\pi\left(r_u\right)^3-\frac{4}{3}\pi\left(\frac{r_t+r_u}{2}\right)^3,$$

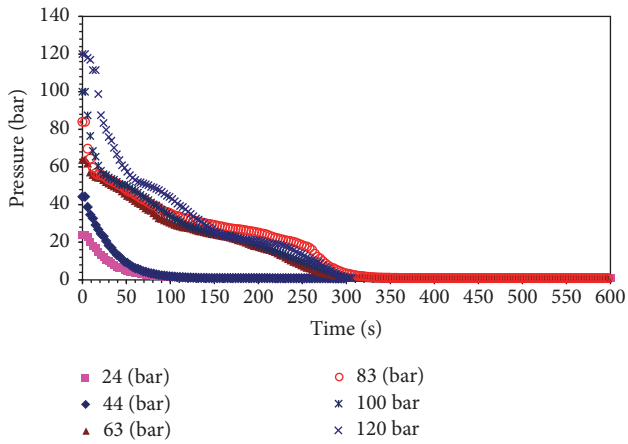

FIGURE 11: Pressure versus time plot for the depressurization experiments at 100°C.

$$\text{Accumulation} = -\text{Flux Out}\times\text{Area},$$

$$\frac{dc_u}{dt}\left[\frac{4}{3}\pi\left(r_u\right)^3-\frac{4}{3}\pi\left(\frac{r_t+r_u}{2}\right)^3\right] = -D_{tu}\frac{\left(c_u-c_t\right)}{\left(r_u-r_t\right)}4\pi\left(\frac{r_t+r_u}{2}\right)^2. \quad (8)$$

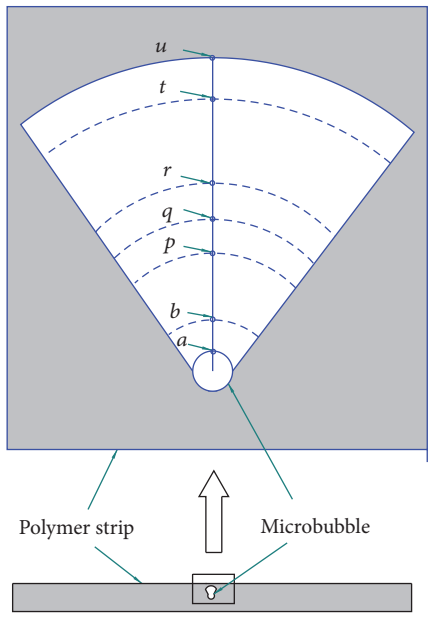

Figure 12: General bubble growth model sketch.

Cancelling π,

$$\frac{dc_u}{dt}\frac{1}{3}\left[(2r_u)^3-(r_t+r_u)^3\right] = -D_{tu}\left(\frac{c_u-c_t}{r_u-r_t}\right)(r_t+r_u)^2. \tag{9}$$

Bubble Surface (Node "a"): Equilibrium Corresponding to Bubble Pressure. The bubble pressure is in equilibrium with the concentration of CO_2 in the polymer at the bubble surface (represented by the concentration at node "a").

$$\begin{aligned} P &= Hc_A, \\ P &= \rho\Re T \Longrightarrow \\ Hc_A &= \rho\Re T. \end{aligned} \tag{10}$$

As P and c_A are linked, the mass balance relating to node "a" should also include the CO_2 in the bubble as well as that in node "a."

The amount (moles, M) of CO_2 associated with node "a" and the bubble is

$$M = V_{\text{node}(a)} \times c_A + V_{\text{bubble}} \times \rho. \tag{11}$$

Hence, the accumulation term for the rate of change of M is

$$\frac{dM}{dt} = V_{\text{node}(a)}\frac{dc_A}{dt} + \rho\frac{dV_{\text{bubble}}}{dt} + V_{\text{bubble}}\frac{d\rho}{dt}. \tag{12}$$

This is equal to the rate at which CO_2 is transported cross the boundary between nodes "a" and "b."

$$\text{Flux} \times \text{Area} = \frac{dM}{dt}, \tag{13}$$

where

$$\begin{aligned} \text{Flux Into Bubble} &= D_{ab}\frac{(c_b-c_a)}{(r_b-r_a)}, \\ \text{Area} &= 4\pi\left(\frac{r_a+r_b}{2}\right)^2, \\ \frac{dM}{dt} &= D_{ab}\frac{(c_b-c_a)}{(r_b-r_a)}4\pi\left(\frac{r_a+r_b}{2}\right)^2. \end{aligned} \tag{14}$$

The molar density of CO_2 in the bubble is given by an Equation of State. At low pressure one can use the Ideal Gas Law $\rho = P/\Re T$, but in general we will use the Soave Redlich Kwong (SRK) Equation of State

$$P = \frac{\Re T}{V-b} - \frac{a}{V(V+b)}. \tag{15}$$

For CO_2, $a = 270485.7$, $b = 0.029683$, $\Re = 8314$ J/kmol-K, P (Pa), T (K), v (m^3/kmol) [21].

An iterative equation for calculating the molar volume for given values of pressure and temperature can be defined as follows:

$$V = b + \frac{\Re T}{P + a/V(V+b)}. \tag{16}$$

The value of molar volume can then be converted into a molar density value.

(a) Model A: Constant Diffusivity, Zero Viscosity. The simplest model (Model A) assumes that bubble growth is only limited by diffusion of gas into the bubble and is not limited by the viscosity of the polymer. The pressure of CO_2 inside the bubble is assumed to be the same as the exterior pressure.

If the exterior (and bubble) pressure varies with time then (12) is used; that is,

$$\begin{aligned} D_{ab}\frac{(c_b-c_a)}{(r_b-r_a)}4\pi\left(\frac{r_a+r_b}{2}\right)^2 &= \left[\frac{4}{3}\pi\left(\frac{r_a+r_b}{2}\right)^3 - \frac{4}{3}\pi r_a^3\right]\frac{dc_a}{dt} + \rho 4\pi r_a^2\frac{dr_a}{dt} + \frac{4}{3}\pi r_a^3\frac{d\rho}{dt} \Longrightarrow \\ dr_a &= \frac{1}{\rho r_a^2}\left[D_{ab}\frac{(c_b-c_a)}{(r_b-r_a)}\left(\frac{r_a+r_b}{2}\right)^2 dt - \left(\frac{1}{3}\left(\frac{r_a+r_b}{2}\right)^3 - \frac{r_a^3}{3}\right)dc_a - \frac{1}{3}r_a d\rho\right]. \end{aligned} \tag{17}$$

(b) Model B: Constant Diffusivity and Viscosity. This model now assumes that the polymer viscosity has an effect on the bubble growth. Diffusion of gas into the bubble now leads to an increase of gas pressure in the bubble; the pressure difference between the inside and outside of bubble then leads to the inflation of the bubble.

This model will first consider the case of constant diffusivity and constant viscosity. First of all, an expression relating the rate of bubble growth to the pressure difference is derived.

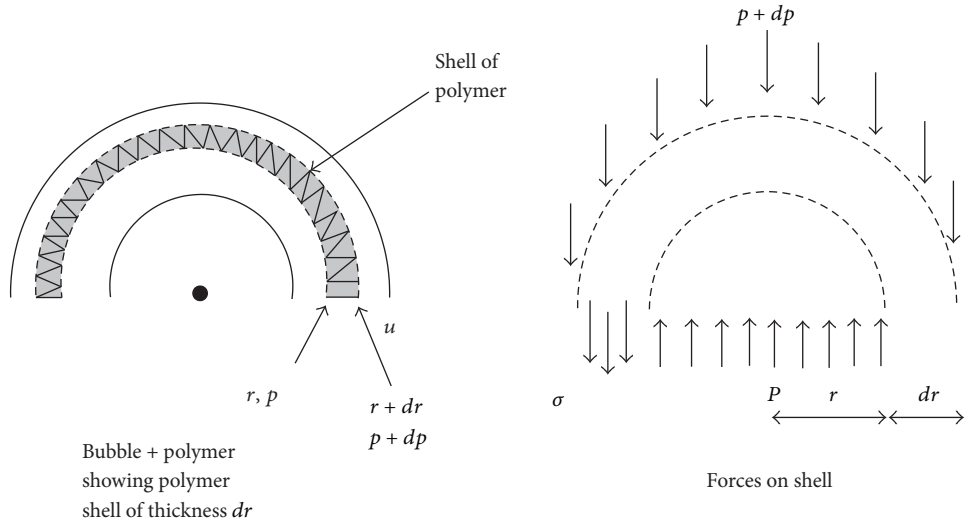

FIGURE 13: Force balance diagram.

A surface tension term is also included to model the pressure drop at the gas/polymer interface due to surface tension. Force balance on a spherical shell element of thickness dr (see Figure 13) is

Inside pressure force

= extensional force in polymer element

+ outside pressure force,

$$\begin{aligned} P\pi r^2 &= \sigma 2\pi r dr + (p+dp)\,\pi\,(r+dr)^2, \\ Pr^2 &= \sigma 2r dr + (p+dp)\,(r+dr)^2, \\ Pr^2 &= \sigma 2r dr + (p+dp)\left(r^2 + 2r dr + dr^2\right), \\ Pr^2 &= 2\sigma r dr + pr^2 + 2prdr + r^2 dp + 2rdrdp. \end{aligned} \tag{18}$$

If $p \ll \sigma$, then $2prdr$ is a negligible term:

$$\begin{aligned} 2\sigma r dr &= -r^2 dp \Longrightarrow \\ 2\sigma dr &= -r dp. \end{aligned} \tag{19}$$

Extensional stress σ is related to extensional strain rate ε' by

$$\sigma = \mu_{\text{ext}}\varepsilon', \quad \left(\varepsilon' = \frac{\dot{r}}{r}\right), \tag{20}$$

where μ_{ext} is the extensional viscosity.

Therefore,

$$2\mu_{\text{ext}}\frac{\dot{r}}{r}dr = -r dp. \tag{21}$$

However, $\dot{r}$ varies with r. Consider a bubble of radius R growing at $\dot{R}$ and a point at radius r moving at $\dot{r}$. The volume between r and R remains constant (see Figure 22).

$$\frac{4}{3}\pi r^3 = \frac{4}{3}\pi R^3 + c. \tag{22}$$

Differentiate with respect to t

$$\begin{aligned} 4\pi r^2\frac{dr}{dt} &= 4\pi R^2\frac{dR}{dt} + 0 \Longrightarrow \\ \dot{r} &= \frac{R^2}{r^2}\dot{R}. \end{aligned} \tag{23}$$

Insert (23) into (21):

$$2\mu_{\text{ext}}\frac{R^2}{r^2}\dot{R}\frac{1}{r}dr = -r dp \tag{24}$$

$$2\mu_{\text{ext}}\frac{R^2\dot{R}}{r^4}dr = -dp. \tag{25}$$

If μ_{ext} is a constant, we can integrate

$$2\mu_{\text{ext}}R^2\dot{R}\int_R^{R_{\text{ext}}}\frac{1}{r^4}dr = \int_{p_b}^{p_{\text{ext}}} -dp, \tag{26}$$

where R_{ext} is the external radius of the polymer sphere

$$\begin{aligned} 2\mu_{\text{ext}}R^2\dot{R}\left[-\frac{1}{3}r^{-3}\right]_R^{R_{\text{ext}}} &= \frac{2\mu_{\text{ext}}R^2\dot{R}}{3}\left[\frac{1}{R^3} - \frac{1}{R_{\text{ext}}^3}\right] \\ &= p_b - p_{\text{ext}}. \end{aligned} \tag{27}$$

Now $\mu_{\text{ext}} = 6\mu$, where μ is shear viscosity [17]

$$4\mu R^2\dot{R}\left[\frac{1}{R^3} - \frac{1}{R_{\text{ext}}^3}\right] = p_b - p_{\text{ext}}. \tag{28}$$

If surface tension forces are significant, then an extra term can be added to reflect this:

$$p_b - p_{\text{ext}} = 4\mu R^2\dot{R}\left[\frac{1}{R^3} - \frac{1}{R_{\text{ext}}^3}\right] + \frac{2\gamma}{R}, \tag{29}$$

where γ is the surface tension [22].

This final equation can be used to calculate the bubble growth rate $\dot{R}$, based on the pressure difference inside the bubble and outside the polymer.

$$\dot{R} = \frac{p_b - p_{\text{ext}} - (2\gamma/R)}{4\mu R^2 \left[1/R^3 - 1/R_{\text{ext}}^3\right]}. \tag{30}$$

In some studies, R_{ext} is considered large compared to R and thus the $1/R_{\text{ext}}^3$ term is regarded as negligible.

The bubble pressure is calculated based on the current size of the bubble and the number of nodes in the bubble and node a.

$$4\pi D_{AB} \frac{(c_b - c_a)}{(r_b - r_a)} \left(\frac{r_a + r_b}{2}\right)^2 = \frac{dM}{dt}, \quad \left(M = c_a V_a + \rho V_{\text{bub}}\right), \tag{31}$$

where V_{bub} is volume of the bubble

Then based on current values for V_{bub} (or R) and M, one can calculate ρ and c_A and p_B from

$$M = c_a V_a + \rho V_{\text{bub}} = \frac{V_a p}{H} + \frac{V_{\text{bub}}}{\nu}, \tag{32}$$

where

$$p_B = \left(\frac{\Re T}{V - b} - \frac{a}{V(V + b)}\right) \quad \text{(Equation of State)} \tag{33}$$

and ν is the mole volume and p_B is the pressure of the bubble.

That is,

$$M = \frac{V_a}{H}\left(\frac{\Re T}{V - b} - \frac{a}{V(V + b)}\right) + \frac{V_{\text{bub}}}{V}. \tag{34}$$

Therefore, the correct value for ν can be found numerically from ρ and c_a.

(c) Model C: Variable Diffusivity and Viscosity. The same general equation for bubble growth can be used as before (25).

$$2\mu_{\text{ext}} \frac{R^2 \dot{R}}{r^4} dr = -dp. \tag{35}$$

However, we now consider the case that viscosity is not a constant.

$$-\int_{p_b}^{p_{\text{ext}}} dp = 2R^2\dot{R}\int_R^{R_{\text{ext}}} \frac{\mu_{\text{ext}}}{r^4} dr = 12R^2\dot{R}\int_R^{R_{\text{ext}}} \frac{\mu}{r^4} dr. \tag{36}$$

In our analysis, we will consider viscosity and diffusivity to vary according to the Williams–Landel–Ferry (WLF) equation, where the local concentration will affect the local glass transition temperature. A similar approach was adopted by Goel and Bechman [8] for modelling viscosity (but not diffusivity) and by Chen et al. [16] who varied both the viscosity and diffusion according to the WLF equation.

The WLF equation is [Williams et al. [23]]

$$\log \frac{\mu}{\mu_o} = \frac{-c_1\left(T - T_g\right)}{c_2 + \left(T - T_g\right)}, \quad \frac{\mu}{\mu_o} = 10^{-c_1(T - T_g)/(c_2 + (T - T_g))} = F, \tag{37}$$

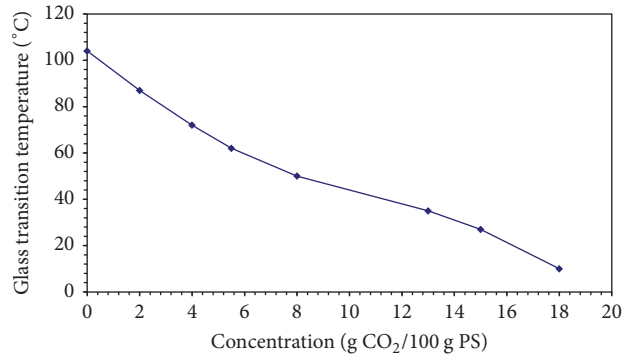

Figure 14: Variation of glass transition temperature of PS with the concentration of CO_2.

where $c_1 = 17.44$, $c_2 = 51.6$ k, and F is a scaling factor arising from the WLF equation.

$$\text{As } D \sim \frac{1}{\mu} \tag{38}$$

[Bird et al. [24]]

$$\frac{D}{D_o} = 10^{(c_1(T - T_g)/(c_2 + (T - T_g)))} = \frac{1}{F}. \tag{39}$$

Now we can say $T_g = T_{g0} - \beta c$ [Condo & Johnston [25]].

β is the slope of the plot of T_g versus concentration

$$\left(T_g = T_{g0} - mp, p = Hc \Longrightarrow \beta = mH\right). \tag{40}$$

These concentration values are plotted against temperature (the glass transition temperature) (see Figure 14). It is clear that T_g decreases with CO_2 concentration.

For each concentration, one can calculate

$$F = 10^{(-c_1(T - T_{g0} + \beta c)/(c_2 + (T - T_{g0} + \beta c)))}, \quad D = \frac{D_0}{F}, \quad \mu = \mu_0 F. \tag{41}$$

For the bubble growth relationship

$$-\int_{p_b}^{p_{\text{ext}}} dp = 2R^2R'\int_R^{R_{\text{ext}}} \frac{\mu_{\text{ext}}}{r^4} dr = 12R^2R'\int_R^{R_{\text{ext}}} \frac{\mu}{r^4} dr \tag{42}$$

as $1/r^4$ varies so dramatically with r it is better to change the variable for integration as per Tuladhar and Mackley [22] paper, $z = 1/r^3$ (m^{-3}).

$p_b - p_{\text{ext}} = 4R^2\dot{R}\int_{z_R}^{z_{\text{ext}}} \mu\, dz = 4R^2\dot{R}\int_{z_R}^{z_{\text{ext}}} F\, dz$, integrated numerically by trapezium rule

$$\dot{R} = \frac{p_b - p_{\text{ext}} - (2\gamma/R)}{4R^2\mu_0\int_{z_R}^{z_{\text{ext}}} F\, dz}. \tag{43}$$

Table 1: Models general parameters values.

Parameters	Values	Source
Initial radius of polymer sphere, $R_{polymer}$ (mm)	1	Assumed
Initial radius of gas bubble, R_{bubble} (mm)	0.01	Measured
Initial pressure, P_i (bar)	24 to 83	Measured
Final pressure, P_f (bar)	1	Measured
Temperature, T (°C)	100	Measured
Density of CO_2 in bubble, ρ (kmol/m^3)	0.032	Calculated
Surface tension, γ (mNm^{-1}), at 1 bar and 200°C	27.7	17
Henry's constant, H (bar), at 70°C	1140.0	Extrapolated
Henry's constant, H (bar), at 100°C	1628.2	30

Table 2: Model B best fit for shear viscosity values and diffusivity values [19].

P_i (bar)	Diffusion coefficient (10^{-10} m^{2}s^{-1})		Best fit for shear viscosity (108 Pa·s)	
	70°C	100°C	70°C	100°C
24	—	0.81	—	0.9
44	—	1.14	—	0.7
63	1.02	1.46	5	0.8
83	1.17	1.67	3.5	0.8

3.8. Discussion of the Model. The set of experiments used to test these models were those with pressure of 24, 44, 63, and 83 bar at a temperature of 70 and 100°C. All these experimental data were logged for 600 sec during depressurization. Each bubble was assumed to be spherical with an initial radius of 0.02 mm and surrounded by a finite volume of polymer. Three bubble growth models were used based on diffusion control only (Model A); constant viscosity and diffusivity (Model B); and varying diffusivity and viscosity according to the WLF equation (Model C). In the models, time zero is taken at the onset of nucleation, which is often sometime after depressurization has commenced and so the starting cell pressure for the model is usually lower than the equilibration pressure (which determines the initial concentration of CO_2 in the polymer). Most of the parameter values such as concentration (c_o), density (ρ), surface tension (γ), viscosity (μ), diffusivity (D), and temperature (T) are either provided or calculated. The general parameter values used in models are shown in Table 1. Each pressure has different diffusivity and shear viscosity as shown in Table 2.

Figures 15 and 16 compare Model A predications with the experimental data of 70 and 100°C for different pressure (24 to 83 bar). The model fit, however, significantly overpredicts bubble growth rates. As we know, Model A assumes that the growth is controlled by diffusion only which lets the growth happen very quickly without any viscous resistance. Therefore, Model B was applied to assess whether a viscous model with surface tension can predict bubble the growth with better accuracy. As we can see in Figures 17 and 18, Model B is better than Model A. This is because this model controls the growth by including viscosity and surface tension, but still the model fit is not good as it predicts a continuously increasing rate of bubble growth. Model C was then applied to determine whether a better prediction could be achieved

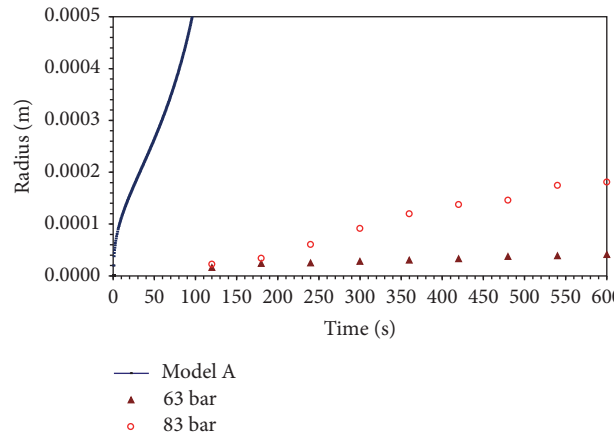

Figure 15: Model A versus experimental data for bubble growth at 70°C.

using a varying viscosity and diffusivity model based on WLF equation.

It is known that variable diffusivity and viscosity model (Model C) can provide realistic estimates of parameters which suggest that diffusion is major influence aspect of the softening of these polymer samples. Model C shows a very reasonable fit with our data by using realistic parameter values; see Table 3. Figures 19 and 20 compare Model C prediction with the experimental data of 70 and 100°C and different pressures (24, 44, 63, and 83 bar), where c_1 = 0.95, c_2 = 32.1 k, Sato et al. [19] and Nikitin et al. [26]. Figure 21 also depicts Model C experimental data for bubble growth at 100°C using WLF equation. This model shows a very reasonable fit with our data by using realistic parameter values and compares Model C prediction with the experimental

Table 3: Model C best fit diffusion coefficient at 100°C.

Pressure (bar)	Concentration of CO_2 (kmol/m^3)	Diffusion coefficient: Sato et al. [19] ($\times 10^{-10}$ m^2/s)	Diffusion coefficient: fit ($\times 10^{-10}$ m^2/s)	Fitting error (error sq)
24	0.37123073	0.81	0.804970412	$2.52968E-05$
44	0.68058968	1.14	1.158677989	0.000348867
63	0.97448068	1.46	1.437437358	0.000509073
83	1.28383962	1.67	1.678843001	$7.81987E-05$

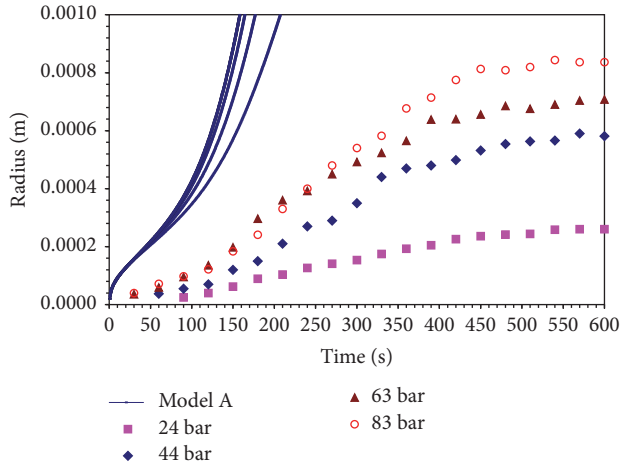

Figure 16: Model A versus experimental data for bubble growth at 100°C.

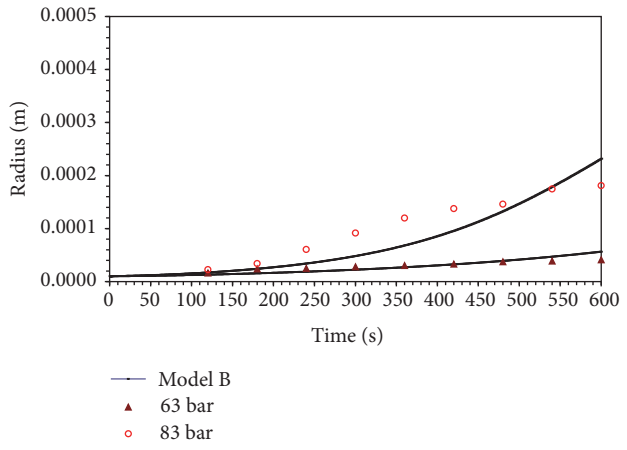

Figure 17: Model B versus experimental data for bubble growth at 70°C.

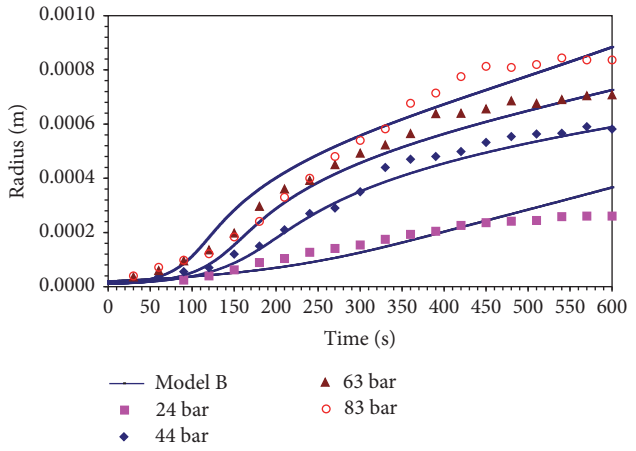

Figure 18: Model B versus experimental data for bubble growth at 100°C.

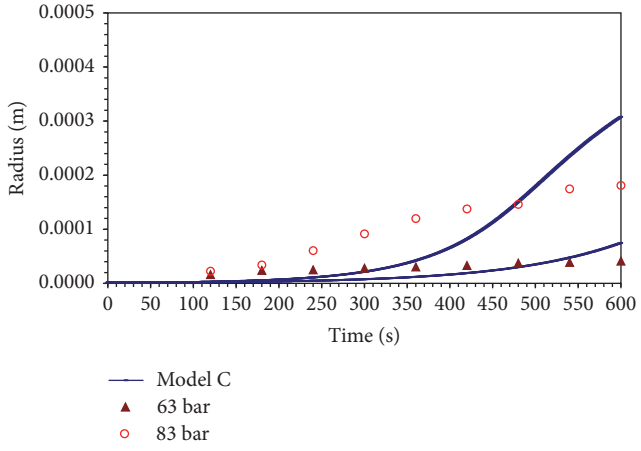

Figure 19: Model C versus experimental data for bubble growth at 70°C.

data of 100°C and different pressures. In general, foaming behavior is controlled by both diffusion and viscosity but these coefficients are varied according to the nature of the polymer.

4. Conclusion

Three sets of experiments were carried out at operating temperatures of 50, 70, and 100°C each over a range of pressures from 24 to 120 bar. For the 100°C experiments, the polymer will be in the rubbery state at the onset of depressurization and much of the subsequent time period. However, most of the 50°C experiments (below 100 bar) will be with the polymer entirely within the glassy state. Images during depressurization at 50°C and with initial pressure up to 83 bar and at 70°C at initial pressure up to 44 bar show no sign of any bubble formation. These correspond to conditions below T_g of PS. The third set of experiments was performed at a higher temperature (100°C) (above T_g of PS) up to 120 bar. The nucleation appeared to occur

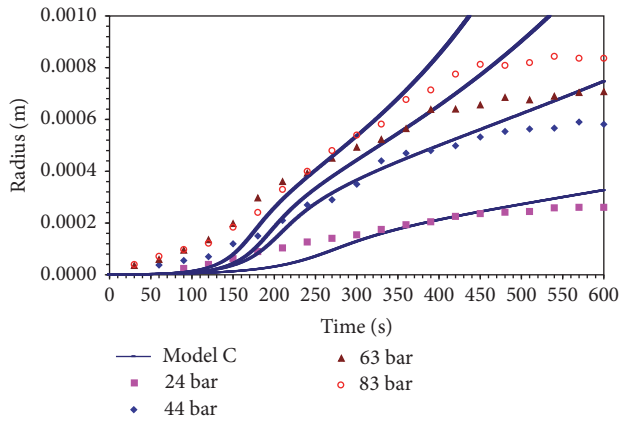

Figure 20: Model C versus experimental data for bubble growth at 100°C.

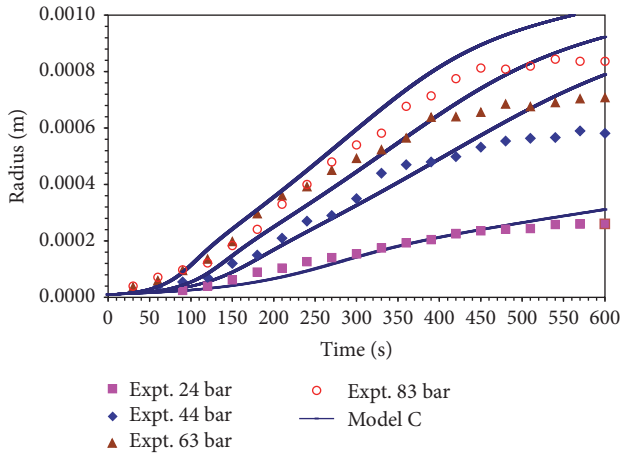

Figure 21: Model C versus experimental data for bubble growth at 100°C using WLF equation.

randomly leading to subsequent bubble growth from these sites, with maximum radius of 0.02–0.83 mm. Bubble growth has been theoretically addressed by number of researchers and most of the models are similar. The expansion occurs by diffusion of a dissolved gas from the supersaturated polymer envelope into the bubble. The main parameters that play the potentially significant role in bubble foaming are viscosity, diffusivity, and surface tension. Three models were applied on the foaming experimental data. Model C was applied to assess the variation of viscosity and diffusivity model with the WLF equation. The model shows very good agreement by using realistic parameter values.

Nomenclature

c: Concentration of CO_2 in the slab (g/ml)
D: Diffusion coefficient (m^2/s)
D_o: Coefficient in WLF equation for diffusivity (m^2/s)
Mw: Molecular weight of the polymer (g/mol)
P: Pressure (bar)

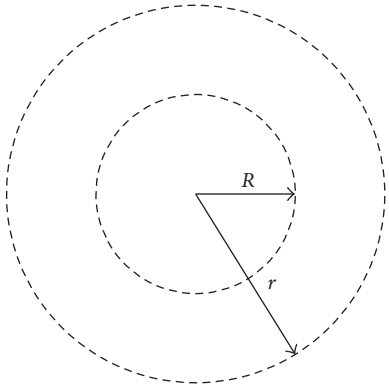

Figure 22

P_i: Initial pressure (bar)
P_f: Final pressure (bar)
H: Henry's constant (bar)
m: Mass of the specimen
R_{polyme}: Initial radius of polymer sphere (mm)
R_{bubble}: Initial radius of gas bubble (mm)
$\mathfrak{R}$: Universal gas constant = 8314 J/kmol-K
r: Radius of a representative bubble (m)
t: Time (sec)
ρ: Polymer density (kg/m^3, k mol/m^3)
μ: Viscosity (shear viscosity) (Pa·s)
μ_o: Viscosity in WLF equation for viscosity (Pa·s)
μ_{ext}: Extensional viscosity (Pa·s)
γ: Surface tension (external stress) (N/m)
σ: Extensional stress
ε': Extensional strain rate
ε_{max}: Strain
β: Side group transition
$V_{polymer}$: Volume of polymer
f: Fraction of polymer volume inside the nodal radius
T: Temperature (K)
b: Width of the sample strips (m)
c: Concentration of CO_2 at time t and distance x into the slab (g/ml)
c_e: Equilibrium concentration in slab (corresponding to infinite time) (g/ml)
D: Diffusion coefficient (m^2/s)
D_o: Coefficient in WLF equation for diffusivity (m^2/s)
M: Moles of CO_2
Mw: Molecular weight of the polymer (kg/kmol)
Mw_{CO2}: Molecular weight of the carbon dioxide (mol/m^3)
P: Pressure (bar)
P_c: Absolute pressure (Mpa)
P_i: Initial pressure (bar)
P_f: Final pressure, (bar)
$\mathfrak{R}$: Gas constant, (8.3145 J/mol K)
r: Radius of a representative bubble (m)

S: Swelling ratio
t: Time (sec)
T_g: Glass transition temperature (°C)
$V_{polymer}$: Polymer volume ($V_{Polymer}$) (m^3)
V_{bub}: Volume of the bubble (m^3)
V_{Rod}: Rod volume (m^3)
V_{Sphere}: Volume of a representative bubble (m^3)
V_i: Volume of the specimen before foaming (m^3)
V_f: Volume of the specimen after foaming (m^3)
ΔV: The difference in the volume
V: Molar volume (m^3)
z: $1/r^3$ (m^{-3}).

Conflicts of Interest

The author declares no conflicts of interest.

Acknowledgments

The author acknowledges the Kuwait Institute for Scientific Research (KISR) for the financial support through Project no. PC 012K.

References

[1] D. L. Tomasko, H. Li, D. Liu et al., "A Review of CO_2 applications in the processing of polymers," *Industrial & Engineering Chemistry Research*, vol. 42, no. 25, pp. 6431–6456, 2003.

[2] J. R. Royer, Y. J. Gay, J. M. Desimone, and S. A. Khan, "High-pressure rheology of polystyrene melts plasticized with CO2: Experimental measurement and predictive scaling relationships," *Journal of Polymer Science Part B: Polymer Physics*, vol. 38, no. 23, pp. 3168–3180, 2000.

[3] A. I. Cooper, "Polymer synthesis and processing using supercritical carbon dioxide," *Journal of Materials Chemistry*, vol. 10, no. 2, pp. 207–234, 2000.

[4] S. Areerat, E. Funami, Y. Hayata, D. Nakagawa, and M. Ohshima, "Measurement and prediction of diffusion coefficients of supercritical CO2 in molten polymers," *Polymer Engineering & Science*, vol. 44, no. 10, pp. 1915–1924, 2004.

[5] C. Drohmann and E. J. Beckman, "Phase behavior of polymers containing ether groups in carbon dioxide," *The Journal of Supercritical Fluids*, vol. 22, no. 2, pp. 103–110, 2002.

[6] H. Tai, C. E. Upton, L. J. White et al., "Studies on the interactions of CO2 with biodegradable poly(dl-lactic acid) and poly(lactic acid-co-glycolic acid) copolymers using high pressure ATR-IR and high pressure rheology," *Polymer Journal*, vol. 51, no. 6, pp. 1425–1431, 2010.

[7] J. J. A. Barry, H. S. Gidda, C. A. Scotchford, and S. M. Howdle, "Porous methacrylate scaffolds: Supercritical fluid fabrication and in vitro chondrocyte responses," *Biomaterials*, vol. 25, no. 17, pp. 3559–3568, 2004.

[8] S. K. Goel and E. J. Beckman, "Nucleation and growth in microcellular materials: supercritical CO2 as foaming agent," *AIChE Journal*, vol. 41, no. 2, pp. 357–367, 1995.

[9] S. K. Goel and E. J. Beckman, "Generation of microcellular polymeric foams using supercritical carbon dioxide. I: effect of pressure and temperature on nucleation," *Polymer Engineering & Science*, vol. 34, no. 14, pp. 1137–1147, 1994.

[10] I. Tsivintzelis, A. G. Angelopoulou, and C. Panayiotou, "Foaming of polymers with supercritical CO_2: an experimental and theoretical study," *Polymer Journal*, vol. 48, no. 20, pp. 5928–5939, 2007.

[11] I. Khan, D. Adrian, and S. Costeux, "A model to predict the cell density and cell size distribution in nano-cellular foams," *Chemical Engineering Science*, vol. 138, pp. 634–645, 2015.

[12] S. Costeux, I. Khan, S. P. Bunker, and H. K. Jeon, "Experimental study and modeling of nanofoams formation from single phase acrylic copolymers," *Journal of Cellular Plastics*, vol. 51, no. 2, pp. 197–221, 2014.

[13] Q. Guo, J. Wang, C. B. Park, and M. Ohshima, "A microcellular foaming simulation system with a high pressure-drop rate," *Industrial & Engineering Chemistry Research*, vol. 45, no. 18, pp. 6153–6161, 2006.

[14] K. Taki, "Experimental and numerical studies on the effects of pressure release rate on number density of bubbles and bubble growth in a polymeric foaming process," *Chemical Engineering Science*, vol. 63, no. 14, pp. 3643–3653, 2008.

[15] J. J. Feng and C. A. Bertelo, "Prediction of bubble growth and size distribution in polymer foaming based on a new heterogeneous nucleation model," *Journal of Rheology*, vol. 48, no. 2, pp. 439–462, 2004.

[16] X. Chen, J. J. Feng, and C. A. Bertelo, "Plasticization effects on bubble growth during polymer foaming," *Polymer Engineering & Science*, vol. 46, no. 1, pp. 97–107, 2006.

[17] M. Amon and C. D. Denson, "A study of the dynamics of foam growth: analysis of the growth of closely spaced spherical bubbles," *Polymer Engineering & Science*, vol. 24, no. 13, pp. 1026–1034, 1984.

[18] T. R. Tuladhar and M. R. Mackley, "The development of polymer foam microstructure: Experimental observations and matching modelling for polystyrene foams using different blowing agents," in *Proceedings of the 7th World Congress of Chemical Engineering (GLASGOW '05)*, pp. 10–14, Institution of Chemical Engineers (IChemE), Glasgow, Scotland, July 2005.

[19] Y. Sato, T. Takikawa, S. Takishima, and H. Masuoka, "Solubilities and diffusion coefficients of carbon dioxide in poly(vinyl acetate) and polystyrene," *The Journal of Supercritical Fluids*, vol. 19, no. 2, pp. 187–198, 2001.

[20] S. Al-Enezi, K. Hellgardt, and A. G. F. Stapley, "Mechanical measurement of the plasticization of polymers by high-pressure carbon dioxide," *International Journal of Polymer Analysis and Characterization*, vol. 12, no. 3, pp. 171–183, 2007.

[21] J. R. Calvert and R. A. Farrar, *An Engineering Data Book*, Palgrave, New York, NY, USA, 1999.

[22] T. R. Tuladhar and M. R. Mackley, "Experimental observations and modelling relating to foaming and bubble growth from pentane loaded polystyrene melts," *Chemical Engineering Science*, vol. 59, no. 24, pp. 5997–6014, 2004.

[23] M. L. Williams, R. F. Landel, and J. D. Ferry, "The temperature dependence of relaxation mechanisms in amorphous polymers and other glass-forming liquids," *Journal of the American Chemical Society*, vol. 77, no. 14, pp. 3701–3707, 1955.

[24] R. B. Bird, W. E. Stewart, and E. N. and Lighrfoot, *Transport phenomena*, Wiley, New York, NY, USA, 1960.

[25] P. D. Condo and K. P. Johnston, "Retrograde vitrification of polymers with compressed fluid diluents: experimental confirmation," *Macromolecules* , vol. 25, no. 24, pp. 6730–6732, 1992.

[26] L. N. Nikitin, M. O. Gallyamov, R. A. Vinokur et al., "Swelling and impregnation of polystyrene using supercritical carbon dioxide," *The Journal of Supercritical Fluids*, vol. 26, no. 3, pp. 263–273, 2003.